Use of a Vertical Vorticity Equation in Variational Dual-Doppler Wind Analysis

ALAN SHAPIRO

School of Meteorology, and Center for Analysis and Prediction of Storms, University of Oklahoma, Norman, Oklahoma

COREY K. POTVIN

School of Meteorology, University of Oklahoma, Norman, Oklahoma

JIDONG GAO

Center for Analysis and Prediction of Storms, University of Oklahoma, Norman, Oklahoma

ABSTRACT

The utility of the anelastic vertical vorticity equation in a weak-constraint (least squares error) variational dual-Doppler wind analysis procedure is explored. The analysis winds are obtained by minimizing a cost function accounting for the discrepancies between observed and analyzed radial winds, errors in the mass conservation equation, errors in the anelastic vertical vorticity equation, and spatial smoothness constraints. By using Taylor's frozen-turbulence hypothesis to shift analysis winds to observation points, discrepancies between radially projected analysis winds and radial wind observations can be calculated at the actual times and locations the data are acquired. The frozen-turbulence hypothesis is also used to evaluate the local derivative term in the vorticity equation. Tests of the analysis procedure are performed with analytical pseudo-observations of an array of translating and temporally decaying counterrotating updrafts and downdrafts generated from a Beltrami flow solution of the Navier–Stokes equations. The experiments explore the value added to the analysis by the vorticity equation constraint in the common scenario of substantial missing low-level data (radial wind observations at heights beneath 1.5 km are withheld from the analysis). Experiments focus on the sensitivity of the most sensitive analysis variable—the vertical velocity component—to values of the weighting coefficients, volume scan period, number of volume scans, and errors in the estimated frozen-turbulence pattern-translation components. Although the vorticity equation constraint is found to add value to many of these analyses, the analysis can become significantly degraded if estimates of the pattern-translation components are largely in error or if the frozen-turbulence hypothesis itself breaks down. However, tests also suggest that these negative impacts can be mitigated if data are available in a rapid-scan mode.

1. Introduction

Use of the vertical vorticity equation in the analysis of vertical motion has a long but sporadic history. Dedebant and Wehrlé (1935) and Sawyer (1949) proposed a synoptic-scale procedure now known as the vorticity method to diagnose the vertical velocity from the vertical vorticity equation (combined with mass conservation) and estimates of the vertical vorticity and its tendency. In this procedure, the horizontal divergence of the wind field is fixed by the requirement that the rate of change of vorticity following the horizontal motion of an air parcel is forced by the stretching of absolute vorticity. The procedure has been applied to synoptic-scale analyses of the height field, assuming geostrophy (Riehl et al. 1952; Eliassen and Hubert 1953; Collins and Kuhn 1954; Nash and Chamberlain 1954; Miller and Panofsky 1958; Fuelberg and Funk 1987), and to high-temporal-resolution wind profiler data (Lee and Browning 1994; Lee et al. 1995). Eliassen and Hubert (1953) also briefly considered a mesoscale form of vorticity equation that included vertical advection and tilting terms, and they noted that, if the horizontal winds were regarded as known, the vertical velocity was governed by a first-order linear partial differential equation whose solution could

Corresponding author address: Alan Shapiro, School of Meteorology, University of Oklahoma, 120 David L. Boren Blvd., Room 5900, Norman, OK 73072.
E-mail: ashapiro@ou.edu

be obtained by the method of characteristics. Mesoscale vertical vorticity equations were later used in vertical velocity analyses by using objectively analyzed upper-air winds in a tropical easterly wave (Yanai and Nitta 1967), horizontal wind data from numerically simulated supercell and microburst-producing storms (Mewes and Shapiro 2002), and dual-Doppler radial wind data in tropical cyclones (Lee et al. 2003, 2006). Several of these synoptic-scale and mesoscale studies suggest that the vorticity methods can be quite sensitive to the temporal resolution of the data.

Only recently, however, have mesoscale vertical vorticity equations been incorporated into multiple-Doppler analyses of all three wind components. In the new approaches, the three wind components are constrained by a vorticity equation, momentum equations, mass conservation equation, radial wind data, and possibly penalty constraints on time and/or space derivatives. Protat and Zawadzki (2000) introduced a wind and thermodynamic retrieval that imposed mass conservation as a strong constraint, the three momentum equations and a mesoscale vertical vorticity equation as weak constraints (approximate, least squares error), a penalty constraint on the time derivatives of the vector wind field, and a linear time interpolation treatment of the observations. The time derivatives were evaluated in a moving reference frame. Although provision for a vorticity equation constraint did not significantly affect the analyzed wind field in tests with radial wind data of a shallow hailstorm sampled by a network of bistatic radars, a markedly improved value of an error-checking parameter indicated that the derivatives of the wind field were improved, thus bolstering confidence in the retrieved thermodynamic fields (both the thermodynamic retrieval and the vorticity equation are derived from the equations of motion). The method was applied by Protat et al. (2001) to a more detailed analysis of that hailstorm. Liu et al. (2005) considered a purely weak-constraint form of wind and thermodynamic retrieval, with each analyzed wind component varying linearly with time, between the start of the first volume scan and the end of the second volume scan, and varying spatially as a product of Legendre polynomial expansions in the three spatial coordinates (as in Scialom and Lemaître 1990). Their tests with numerically simulated data of a supercell storm showed that a mesoscale vertical vorticity equation constraint could significantly improve the accuracy of the retrieved vertical velocity and temperature fields.

In this study, we further explore the utility of the vertical vorticity equation as a constraint in the dual-Doppler analysis of the three wind components. Our focus is on the value added by the vorticity equation in a problem of long-standing interest in the radar and mesoscale meteorology communities: improving the accuracy of vertical velocity estimates, especially in cases of substantial missing low-level data [see discussions on the vertical velocity problem in Mewes and Shapiro (2002) and references therein]. Scan geometries typically dictate that the vertical velocity w is the least well observed of the velocity components and is thus the most difficult component to accurately synthesize. In traditional dual-Doppler analysis, a mass conservation equation is imposed along with the requirement that the component of the velocity vector normal to the ground vanish at the ground (impermeability condition). A kinematic storm-top condition is sometimes imposed in place of (or in addition to) this condition. In the general case where the topographic height is given by $z = f(x, y)$, the impermeability condition constrains the vertical velocity field at the ground to satisfy $w = u\partial f/\partial x + v\partial f/\partial y$ (u, v, and w are the velocity components associated with the Cartesian coordinates x, y, and z, respectively). In the special case where the ground is flat, this condition reduces to $w = 0$. Unfortunately, because of the earth's curvature, nonzero elevation angle of the lowest radar beam, ground clutter contamination, and beam blockage, data voids hundreds to thousands of meters thick commonly separate the lower surface of data coverage from the earth's surface, where the impermeability condition could legitimately be applied. The problem of missing low-level data is especially acute for radars operating in mountainous terrain.

The analysis technique explored here is similar to the weak-constraint variational procedure of Gao et al. (1999), although here a vertical vorticity equation is incorporated into the analysis. The vorticity equation constraint is similar to that of Protat and Zawadzki (2000), Protat et al. (2001), and Liu et al. (2005); although in our procedure, the frozen-turbulence hypothesis is invoked to rewrite the time derivative term (tendency) in terms of spatial derivative terms. Conceptually, this is equivalent to neglecting time derivatives in a moving reference frame.

In the remainder of the paper, we discuss the anelastic vertical vorticity equation and our treatment of its time derivative term (section 2), present the variational wind analysis procedure (section 3), and describe an analytical Beltrami flow solution of the Navier–Stokes equations used to generate pseudo-observations for testing the analysis procedure (section 4). The particular flow considered is a translating temporally decaying array of counterrotating updrafts and downdrafts. The parameter values controlling the pseudo-observations, the characteristics of the virtual radars, the analysis grid, and the weighting coefficients in the analysis procedure

are specified in section 5. Results from data denial experiments (missing low-level data) are presented in section 6, with a focus on the length of the analysis time window (radar scan period and number of volume scans). Conclusions follow in section 7.

2. Anelastic vertical vorticity equation

We consider the governing equations for a compressible atmosphere under an anelastic approximation as given in Dutton and Fichtl (1969), Lipps and Hemler (1982), and Bannon (1996). These equations are commonly used to study a variety of small-scale and mesoscale phenomena, including deep moist convective storms. For our purposes, we need only consider the mass conservation equation and the horizontal components of the equations of motion,

$$\frac{\partial(\rho_s u)}{\partial x} + \frac{\partial(\rho_s v)}{\partial y} + \frac{\partial(\rho_s w)}{\partial z} = 0, \tag{1}$$

$$\frac{\partial u}{\partial t} + u\frac{\partial u}{\partial x} + v\frac{\partial u}{\partial y} + w\frac{\partial u}{\partial z} = -\frac{\partial \pi}{\partial x}, \quad \text{and} \tag{2}$$

$$\frac{\partial v}{\partial t} + u\frac{\partial v}{\partial x} + v\frac{\partial v}{\partial y} + w\frac{\partial v}{\partial z} = -\frac{\partial \pi}{\partial y}, \tag{3}$$

where u and v are the horizontal velocity components, w is the vertical velocity component, ρ_S is a height-dependent base-state density, and π is the perturbation pressure divided by ρ_S. We omit Coriolis terms in (2) and (3) because the rotation period for the earth is much larger than the time window over which the dual-Doppler analysis is to be performed. Our omission of diffusion/mixing terms in (2) and (3) is less justifiable, but the impact of their omission is mitigated by our use of these equations (or rather the vorticity equation derived from them) as a weak constraint rather than as a strong constraint. In any case, in principle, one may include Coriolis and explicit diffusion/mixing terms in (2) and (3), as in Protat and Zawadzki (2000) or Liu et al. (2005).

Subtracting the y derivative of (2) from the x derivative of (3) yields the vorticity equation

$$\frac{\partial \zeta}{\partial t} + u\frac{\partial \zeta}{\partial x} + v\frac{\partial \zeta}{\partial y} + w\frac{\partial \zeta}{\partial z} + \left(\frac{\partial v}{\partial z}\frac{\partial w}{\partial x} - \frac{\partial u}{\partial z}\frac{\partial w}{\partial y}\right)$$
$$+ \zeta\left(\frac{\partial u}{\partial x} + \frac{\partial v}{\partial y}\right) = 0, \tag{4}$$

where ζ $(\equiv \partial v/\partial x - \partial u/\partial y)$ is the vertical vorticity. Equation (4) provides a relation between the three velocity components unencumbered by the presence of thermodynamic variables. The absence of baroclinic terms

in this equation and their negligibility in other mesoscale vertical vorticity equations were noted in the radar meteorology community many years ago (e.g., Ray 1976; Heymsfield 1978). Although the baroclinic vector is dynamically significant in thunderstorms, density currents, gravity waves, and other mesoscale phenomena, it points mostly in the horizontal and thus serves primarily to generate horizontal vorticity, not vertical vorticity.

A challenge with the use of (4) in dual-Doppler wind analysis is the treatment of the time derivative term. In one approach, data from at least two successive volume scans from each radar are used to discretize the time derivative as a finite difference across the scan interval. The accuracy of that approach should be acceptable if the time scale of the flow is sufficiently longer than the scan period of the radars, but large errors can be expected otherwise. Flow unsteadiness is often partitioned conceptually into categories of translation and evolution, although in practice such a partitioning may not be straightforward or appropriate. The notion of translation underpins the use of space-to-time conversions ubiquitous in data analysis, and is described by Taylor's (1938) frozen-turbulence hypothesis: "If the velocity of the air stream which carries the eddies is very much greater than the turbulent velocity, one may assume that the sequence in changes in u at the fixed point are simply due to the passage of an unchanging pattern of turbulent motion over the point . . . ." This can be quantified as

$$\frac{\partial}{\partial t} = -U\frac{\partial}{\partial x} - V\frac{\partial}{\partial y}, \tag{5}$$

where U and V are pattern-translation components. Temporal-discretization errors arising from translation can be mitigated by discretizing the time derivative in a frame of reference moving with the pattern. Objective methods to calculate U, V from radar data include cross-correlation analysis (Zawadzki 1973; Austin and Bellon 1974; Anagnostou and Krajewski 1999) and minimization of a cost function in which a frozen-turbulence constraint is imposed (Gal-Chen 1982; Chong et al. 1983; Shapiro et al. 1995; Caillault and Lemaître 1999; Liou and Luo 2001; Lazarus et al. 2001; Matejka 2002; Caya et al. 2002; Liu et al. 2004; and many others). In contrast, temporal-discretization errors associated with changes in the intensity and/or shape of a pattern (i.e., evolution effects) cannot be mitigated by the use of a moving reference frame.

A second approach to evaluating the time derivative term in (4), one that we apply in this study, is to use (5) to replace the time derivative term with spatial derivative terms. Advantages of this approach are that pattern translation can be accounted for in a fixed reference

frame and that the time derivative term can be evaluated with data from only a single volume scan from each radar. However, large errors in the estimation of that term can be expected if evolution effects become important or if the pattern-translation components are poorly estimated.

3. Analysis procedure

A weak-constraint variational formalism is applied to the analysis of the Cartesian wind components (u, v, w) on a Cartesian grid (x, y, z) using radial wind observations from two Doppler radars. In this weak-constraint procedure, we seek analysis wind fields that 1) minimize the squared discrepancies between the observed radial winds and the radial projections of the analysis wind vectors, and 2) approximately satisfy (least squares error sense) mass conservation and vorticity equation constraints. Spatial smoothness penalty terms are also imposed. A cost function J accounting for the sum of the squared discrepancies/errors is introduced, and an iterative minimization algorithm is used to obtain the analysis wind fields that minimize J. We consider weak constraints rather than strong (exactly satisfied) constraints because the constraining relations have a variety of errors, uncertainties, and limitations associated with them, including temporal-discretization errors and neglect of diffusion/mixing terms in the vorticity equation, spatial-discretization errors in the mass conservation and vorticity equations, observational errors in the radial velocity data, and spatiotemporal interpolation errors in our treatment of the analyzed radial velocity fields. The general framework of weak-constraint analysis is described in Sasaki (1970), Daley (1991), and other standard references. The specific procedure considered here is perhaps most similar to the variational methods of Gao et al. (1999), Protat and Zawadzki (2000), Protat et al. (2001), or Liu et al. (2005), although with some differences in the forms or implementations of some of the constraints.

During each iteration, radial wind observations are compared with the corresponding radial projections of the analysis wind vectors and the discrepancies are noted. This comparison requires some careful technical considerations. The discrepancies are estimated at the times and locations of the observations, with standard transformation formulas used to obtain the Cartesian coordinates of an observation point from the coordinates of that point in its native spherical coordinate system (e.g., appendix C of Shapiro et al. 1995). Although the analysis winds will be output from the procedure at a single time ($t = 0$), they are available (via the frozen-turbulence constraint) for the discrepancy cal-

culation during a time window extending over at least one radar volume scan period. The frozen-turbulence constraint (5) yields functional relations for the analysis wind components u^a, v^a, and w^a as

$$u^a(x, y, z, t) = u^a(x - Ut, y - Vt, z, 0),$$
$$v^a(x, y, z, t) = v^a(x - Ut, y - Vt, z, 0), \quad \text{and}$$
$$w^a(x, y, z, t) = w^a(x - Ut, y - Vt, z, 0), \quad \text{respectively.}$$
$$\tag{6}$$

In view of (6), an analysis wind component evaluated at an observation time $t*$ at an observation point $(x*, y*, z*)$ is equal to the same analysis wind component evaluated at time 0 at the shifted location $(x* - Ut*, y* - Vt*, z*)$. A spatial interpolation of the analysis winds from the analysis grid points to the shifted location is performed with a three-dimensional isotropic (spherical) Cressman analysis (Haltiner and Williams 1980).

With the coordinates of the first radar (Rad1) denoted by (x_1, y_1, z_1), the projection of the analysis wind vector at an observation point $(x*, y*, z*)$ in the direction of Rad1 is given by

$$v_{r1}^a = \frac{1}{r_1} \{ (x* - x_1) u^a(x*, y*, z*, t*)$$
$$+ (y* - y_1) v^a(x*, y*, z*, t*)$$
$$+ (z* - z_1)[w^a(x*, y*, z*, t*) - |w_t|] \}, \quad (7)$$

where r_1 is the distance of the observation point from Rad1:

$$r_1 = \sqrt{(x* - x_1)^2 + (y* - y_1)^2 + (z* - z_1)^2}. \quad (8)$$

The Cartesian analysis wind components in (7) are evaluated with the shifting/interpolation procedure described above. Analogous equations define v_{r2}^a, the projection of the analysis wind vector in the direction of the second radar (Rad2), and r_2, the distance of an observation point from Rad2. The terminal velocity w_t is included in (7) to account for the mismatch between the air velocity and the velocity of the radar scatterers. Hydrometeor scatterers fall with a vertical velocity component w_t relative to the air but are otherwise relatively faithful markers of air motion [see Dowell et al. (2005) and Shapiro (2005) for exceptions and discussions of this point]. The terminal velocity of hydrometeors is commonly parameterized in terms of the radar reflectivity factor (e.g., appendix B of Shapiro et al. 1995).

The mismatch between the observed radial wind components from the two radars, v_{r1}^{obs} and v_{r2}^{obs}, and the

corresponding analyzed/shifted/projected winds, v_{r1}^a and v_{r2}^a, can be quantified by the cost function

$$J_O \equiv \sum_{\text{Rad1}} \lambda_{O1} r_1^2 (v_{r1}^{\text{obs}} - v_{r1}^a)^2 + \sum_{\text{Rad2}} \lambda_{O2} r_2^2 (v_{r2}^{\text{obs}} - v_{r2}^a)^2,$$

(9)

where the sums extend over the observation grid points of the Rad1 and Rad2 radars over a time window of at least one volume scan period. An extension of (9) to three or more radars is straightforward. Range-weighting factors r_1^2 and r_2^2 are included in (9) to account for the fact that radial wind observations are not strictly point measurements but represent probe volumes that grow as the square of the distance from the radar. The weights λ_{O1} and λ_{O2}, along with other constraint weights, will be treated as constants. A similar observational constraint appears in Gao et al. (1999), Protat and Zawadzki (2000), Protat et al. (2001), and Liu et al. (2005), though in the idealized experiments in Gao et al. (1999) the radial wind observations were considered to be simultaneous, and in Liu et al. (2005) the analyzed winds are brought to the observation time through linear time interpolation rather than through a frozen-turbulence shift.

The extent to which the analysis wind field violates the anelastic mass conservation Eq. (1) is quantified by the cost function

$$J_M \equiv \sum_{\text{Cart}} \lambda_M \left[\frac{\partial(\rho_s u^a)}{\partial x} + \frac{\partial(\rho_s v^a)}{\partial y} + \frac{\partial(\rho_s w^a)}{\partial z} \right]^2, \quad (10)$$

where the sum extends over all the analysis points on the Cartesian analysis grid (Cart). The base-state density $\rho_S(z)$ can be obtained from a nearby sounding or approximated with an exponential function (e.g., Ray et al. 1975; Doviak et al. 1976; Scialom and Lemaître 1990).

The extent to which the analysis wind field violates the anelastic vertical vorticity Eq. (4) is quantified by the cost function

$$J_V \equiv \sum_{\text{Cart}} \lambda_V \left[(u^a - U) \frac{\partial \zeta^a}{\partial x} + (v^a - V) \frac{\partial \zeta^a}{\partial y} + w^a \frac{\partial \zeta^a}{\partial z} \right.$$
$$\left. + \left(\frac{\partial v^a}{\partial z} \frac{\partial w^a}{\partial x} - \frac{\partial u^a}{\partial z} \frac{\partial w^a}{\partial y} \right) + \zeta^a \left(\frac{\partial u^a}{\partial x} + \frac{\partial v^a}{\partial y} \right) \right]^2,$$

(11)

where we have used (5) to replace the time derivative term by spatial derivative terms.

Finally, we introduce a cost function associated with first-derivative spatial smoothness penalty terms:

$$J_S \equiv \sum_{\text{Cart}} \lambda_{S1} \left[\left(\frac{\partial u^a}{\partial x} \right)^2 + \left(\frac{\partial u^a}{\partial y} \right)^2 + \left(\frac{\partial v^a}{\partial x} \right)^2 + \left(\frac{\partial v^a}{\partial y} \right)^2 \right]$$
$$+ \sum_{\text{Cart}} \lambda_{S2} \left[\left(\frac{\partial u^a}{\partial z} \right)^2 + \left(\frac{\partial v^a}{\partial z} \right)^2 \right]$$
$$+ \sum_{\text{Cart}} \lambda_{S3} \left[\left(\frac{\partial w^a}{\partial x} \right)^2 + \left(\frac{\partial w^a}{\partial y} \right)^2 \right] + \sum_{\text{Cart}} \lambda_{S4} \left(\frac{\partial w^a}{\partial z} \right)^2.$$

(12)

These terms act as low-pass filters for noise suppression and also provide smooth interpolation of analysis variables across data voids. Sasaki (1970, 1971) advocated the use of first-derivative penalty terms, whereas Wahba and Wendelberger (1980) and Thacker (1988) advocated the use of second-derivative (Laplacian) terms. Wahba and Wendelberger's (1980) concern with first-derivative penalty terms stemmed from the presence of a singularity in the Green's function in Sasaki's (1971) solution of the Euler–Lagrange equation arising from minimization of those terms. However, as noted by Sasaki (1971), although the singularity could complicate numerical evaluation of the Green's function solution, in practice the Euler–Lagrange equation could be solved numerically without the need to consider the explicit Green's function solution. In other words, the difficulty was computational, not theoretical. In support of that assessment, we note that singular Green's functions appear in solutions to many classical problems in electrostatics, heat conduction, wave propagation, and mechanics and that special numerical algorithms are available to evaluate singular integrals. Our choice to use a first-derivative penalty constraint was guided by the slightly simpler form of that constraint, as well as the better results with a first-derivative constraint reported by Qiu and Xu (1996) in single-Doppler velocity retrieval experiments with high-resolution data of a microburst. We also considered a simple thought experiment in which penalty-term minimization is used to interpolate data across a data void. Minimizing squared first-derivative terms over the void leads to Laplace's equation, which has the desirable property that the analyzed variable has a maximum or minimum on the data surface bounding the void but not within the void, whereas minimization of a squared Laplacian leads to the biharmonic equation, which permits extrema within the data void (analogous to flexural bulge of thin elastic plates). However (as pointed out by one of the reviewers), an advantage of a second-order spatial smoothness constraint is that its gain curve (ratio of RMS retrieved velocities to RMS real velocities plotted as a function of wavelength) has a sharper cutoff than the corresponding gain curve of the first-order smoothness

constraint. Accordingly, it is harder to separate the unresolved and resolved wavelengths in the first-order procedure. We will compare second-order smoothness results with first-order smoothness results in a future study.

In the current analysis procedure, no background wind field constraint is imposed [although our smoothness constraint can be viewed as a kind of background constraint; as shown by Xu (2005), a background term can be expressed as a smoothness penalty term in which a differential operator acts on a field of analysis increments]. Background winds can, in principle, be estimated from conventional surface observations, nearby soundings, forecast fields from a numerical weather prediction model, or winds obtained from traditional single-Doppler radar algorithms such as velocity–azimuth display (VAD), volume velocity processing (VVP; Doviak and Zrnic 1984), or extended VVP approaches (Caya et al. 2002). However, we believe there is sufficient interest in stand-alone dual-Doppler wind analysis techniques to omit such a constraint in our investigation. In any case, should one want to impose such a constraint, it would be a simple matter to account for it (Gao et al. 1999).

In addition to imposing the weak constraints, we also have the option to impose the impermeability condition at ground level (w is set to zero at ground level in the experiments in which the impermeability option is activated). Although we have not made provision for the vertical velocity to vanish at storm top, such a modification could be made within the present framework. On the other hand, because vertical velocities at storm top can be substantial in cases of rapid storm development, the decision to impose a storm-top condition may not be straightforward.

The goal of our analysis is to determine the u^a, v^a, and w^a analysis fields (control variables) that minimize the sum of the constraints described above; that is, to minimize J, defined by

$$J \equiv J_O + J_M + J_V + J_S, \qquad (13)$$

with w set to zero at ground level in the subset of experiments in which the impermeability condition is imposed. The relative magnitudes of the weighting coefficients λ_{O1}, λ_{O2}, λ_M, λ_V, λ_{S1}, λ_{S2}, λ_{S3}, and λ_{S4} in (9)–(12) determine the relative importance of the individual constraints in (13). The selection of these weights is an important and challenging aspect of variational analysis (Hoffman 1984). In principle, the weights should be chosen so that the individual terms in the cost function have the same order of magnitude. In practice, however, uncertainties in observation errors and equation errors make such weight estimations difficult. Accordingly, as in Hoffman (1984), Xu et al. (1995, 2001), Gao et al. (1999), and Liu et al. (2005), we view the weights as tuning parameters whose values can be determined through experimentation. A set of values will be deemed acceptable if large changes in those values (say, over a 10-fold range) produce relatively small changes in the most sensitive analysis variable, which is the vertical velocity field.

We minimize J with an iterative procedure similar to that of Gao et al. (1999) and Liu et al. (2005). The procedure is initialized with first guesses of zero for all the control variables. During each iteration, provisional values of the control variables are used to calculate J and its derivatives with respect to the control variables. The control variables are then updated using the Polak–Ribiere conjugate gradient method (Press et al. 1992). Every 10 iterations, the updated vertical velocity field is compared to the vertical velocity field from the 10th previous iteration. We consider the procedure to have converged when the change in the vertical velocity is less than a prescribed tolerance (0.02 m s^{-1}) at every analysis point. For most of the experiments conducted in this study, about 1000–1500 iterations were sufficient for convergence. Although this number is rather large, our prescribed tolerance is probably much more stringent than one would need in real applications.

4. Pseudo-observations: An analytical dataset

The analysis procedure is tested in section 6 with analytical data of a three-dimensional Beltrami flow sampled by two virtual Doppler radars. Beltrami flows are a class of exact solutions of the incompressible Navier–Stokes equations in which the vorticity field is aligned with the velocity field (Truesdell 1954; Irmay and Zuzovsky 1970). For the purpose of constructing a flow that offers at least a qualitative resemblance to the motion in deep moist convective systems, we consider the particular Beltrami flow used by Shapiro (1993) in a validation test of the Advanced Regional Prediction System (ARPS), a nonhydrostatic numerical weather prediction model. That flow is characterized by a spatially periodic temporally decaying array of counterrotating updrafts and downdrafts. The flow satisfies the impermeability condition ($w = 0$ at ground level) but satisfies neither the no-slip condition nor the free-slip condition. It is easy to show that the maximum horizontal convergence and divergence of the wind field occur at ground level. Accordingly, in the experiments of section 6, where low-level data are withheld, the largest convergence or divergence signatures do not enter the analysis. These data-denial experiments emulate the common scenario where radars fail to sample strong low-level convergent or divergent flows, for example, at the base of a convective storm updraft, at the leading edge of a density current, in the lower part of a microburst, or in the rear flank downdraft of a supercell.

The velocity field used in the pseudo-observation experiments consists of a Beltrami flow superimposed on an environmental wind with constant x and y wind components, U and V, respectively. In order for this composite flow to satisfy the Navier–Stokes equations exactly, we replace x and y in the formulas used by Shapiro (1993) by $x - Ut$ and $y - Vt$, respectively. The resulting flow is given by

$$u = U - \frac{A}{k^2 + l^2} \{\Lambda l \cos[k(x - Ut)] \sin[l(y - Vt)] \sin(mz) + mk \sin[k(x - Ut)] \cos[l(y - Vt)] \cos(mz)\} \exp(-\nu\Lambda^2 t),$$

$$(14)$$

$$\nu = V + \frac{A}{k^2 + l^2} \{\Lambda k \sin[k(x - Ut)] \cos[l(y - Vt)] \sin(mz) - ml \cos[k(x - Ut)] \sin[l(y - Vt)] \cos(mz)\} \exp(-\nu\Lambda^2 t),$$

and $$(15)$$

$$w = A \cos[k(x - Ut)] \cos[l(y - Vt)] \sin(mz) \exp(-\nu\Lambda^2 t),$$

$$(16)$$

where k, l, and m are the wavenumber components in the x, y, and z directions, respectively, and $\Lambda \equiv \sqrt{k^2 + l^2 + m^2}$ is the wavenumber magnitude. The parameter A is the peak vertical velocity. As is evident from the exponential terms, the spatial pattern undergoes a temporal decay with an e-folding decay time of $T_e \equiv 1/(\nu\Lambda^2)$, where ν is the kinematic viscosity coefficient. If one wanted to consider the artifice of a negative viscosity coefficient, the temporal behavior would be of growth rather than of decay.

Technically, this composite flow is no longer a bona fide Beltrami flow (vorticity vectors are no longer aligned with the velocity vectors), but it does still satisfy the incompressible Navier–Stokes equations exactly. In the interest of brevity, we will still refer to it as a Beltrami flow.

5. Parameter settings for pseudo-observation experiments

In this section, we summarize the parameter values used to define the analysis grid, the characteristics of the virtual radars, the specific Beltrami flow used to generate the pseudo-observations, and the errors imposed on the pseudo-observations. Although there are similarities between the analysis and input-data model constraints, there are also important differences that help mitigate an identical twin problem. Attention will be drawn to these differences.

Pseudo-observations are obtained by taking the radial projections of a velocity field satisfying (14)–(16) with a vertical wavelength of 12 km [$m = 2\pi/(12 \text{ km}) \cong 5.24 \times 10^{-4} \text{ m}^{-1}$], a wavelength in the x and y directions of 10 km [$k = l = 2\pi/(10 \text{ km}) \cong 6.28 \times 10^{-4} \text{ m}^{-1}$ and $\Lambda \cong 1.03 \times 10^{-3} \text{ m}^{-1}$], an e-folding decay time of $T_e = 10$ min, a peak vertical velocity of $A = 10 \text{ m s}^{-1}$, and environmental wind components of $U = V = 10 \text{ m s}^{-1}$. The horizontal wind vectors at the height $z = 1$ km above ground level (AGL; with the environmental winds subtracted off) are displayed in Fig. 1. The flow at this level is notably divergent/convergent and rotational. The horizontal divergence and vertical vorticity fields obtained from (14) and (15) show that the flow at ground level ($z = 0$) is purely divergent/convergent, whereas the flow at $z = 3$ km is purely rotational.

The pseudo-observations are sampled from two virtual radars spaced 40 km apart (Fig. 2). Each radar scans a sequence of 23 elevation angles with a 1.0° elevation angle spacing starting from the lowest elevation angle of 1.1°. The radars scan the same 90°-wide azimuthal sector with 1.0° azimuthal spacing and 200-m-range gate spacing. Experiments are conducted with volume scan periods ranging from 1 to 5 min, although most of the results are presented for the 2-min scan period. In all experiments considered here, the two radars scan in a coordinated manner, with the lowest scans starting at a common time. However, additional experiments with uncoordinated scan strategies (not shown) revealed that the analysis results are not very sensitive to scan time offsets as long as the offsets are small (<1 min).

The analysis domain is a square box (cuboid) with sides of 20-km length in the horizontal, and 6 km in the vertical. The grid spacing is 500 m in the x, y, and z directions. At ground level, the center of the analysis domain is equidistant from the two radars and 20 km north of the radars, which puts the center of the domain about 28 km away from each of the radars (Fig. 2). The radius of influence in the Cressman interpolation step used in the evaluation of J_O is 500 m.

In all experiments, we take the base-state density to be constant and omit the terminal velocity correction in the data constraint (7). As can readily be shown from scale analysis, the geometric contribution of the terminal velocity correction term to the radial wind is small for small
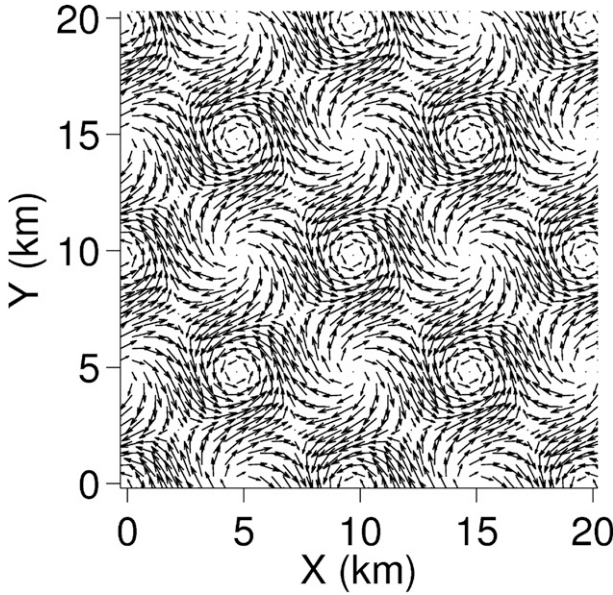
FIG. 1. Horizontal velocity vectors at $z = 1$ km for the Beltrami flow used to generate the pseudo-observations. In this plot, the environmental winds have been subtracted from the full wind vectors to make the convergent/divergent and rotational flow signatures more evident.

elevation angles [also see discussion in Kropfli and Miller (1976)]. We have further verified that such a term would not be significant in our case by performing an experiment in which the vertical velocity term itself was explicitly set to zero in (7); in this experiment, the retrieved vertical velocity field changed by only a few percent.

In the experiments considered in section 6, the two data constraint weights are set equal to each other, $\lambda_{O1} = \lambda_{O2}(=\lambda_O)$, and the four smoothness weights are set equal to each other, $\lambda_{S1} = \lambda_{S2} = \lambda_{S3} = \lambda_{S4}(=\lambda_S)$. To aid with the tuning process, the weights can be rewritten in terms of products of nondimensional tuning parameters and factors that depend on the number of radar observation points (N_1, N_2), the number of analysis points (N_{Cart}), and the characteristics of the observed radial wind field [including the spatial gradient (SG) calculated on the observation grid]:

$$\lambda_O = C_O \left[\sum_{\text{Rad1}} r_1^2 (v_{r1}^{\text{obs}})^2 + \sum_{\text{Rad2}} r_2^2 (v_{r2}^{\text{obs}})^2 \right]^{-1},$$

$$\lambda_M = C_M [N_{\text{Cart}} \overline{\rho}_s (\text{SG})^2]^{-1},$$

$$\lambda_V = C_V [N_{\text{Cart}} (\text{SG})^4]^{-1},$$

$$\lambda_S = C_S [N_{\text{Cart}} (\text{SG})^2]^{-1}, \quad \text{and}$$

$$\text{SG} \equiv \sqrt{\frac{1}{N_1 + N_2} \left[\sum_{\text{Rad1}} \left(\frac{1}{r_1} \frac{\partial v_{r1}^{\text{obs}}}{\partial \theta} \right)^2 + \sum_{\text{Rad2}} \left(\frac{1}{r_2} \frac{\partial v_{r2}^{\text{obs}}}{\partial \theta} \right)^2 \right]}.$$
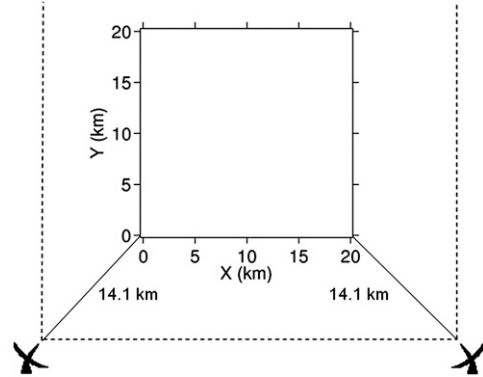
$$(17)$$

FIG. 2. Radar placement and analysis domain (inner square). Dashed lines encompass the 90°-wide azimuthal sectors scanned by each radar.

In this manner, each of the individual J terms in (13) has the same dimensions, and the nondimensional tuning parameters C_O, C_M, C_V, and C_S control the relative influence of the constraints. The tuning parameters used in the majority of the experiments presented in section 6 were set at $C_O = 1$, $C_M = 0.1$, $C_V = 7.0 \times 10^{-4}$, and $C_S = 5.6 \times 10^{-5}$. The values of C_O, C_M, C_V, and C_S were varied from these default settings in a series of sensitivity experiments, which are also described in section 6.

We ran experiments (not shown) comparing the sensitivity of the retrievals to the presence of the r^2 factors in (9) and in the expression for λ_O in (17). Results from experiments in which the r^2 factors were excluded differed little from the experiments in which they were retained (differences on the order of 1% for w and 0.25% for u and v). Presumably, the relatively small size of the analysis grid used in our experiments was a factor in this insensitivity. For all results shown in section 6, these r^2 factors were not included.

Once the radial winds are generated, they are contaminated with Gaussian noise based on a polar form of the Box–Muller method (Press et al. 1992). Using this procedure, random observational errors were simulated with magnitudes up to 15% of the true radial wind values (local, not RMS) and with the first standard deviation of the percent error distribution corresponding to 10% of the true radial wind values. As an additional source of error, the values of the U and V pattern-translation components used in most of the experiments differ systematically from the U and V used to generate the pseudo-observations by 20% (8 and 12 m s^{-1} compared to 10 and 10 m s^{-1}, respectively). In a few experiments, these systematic errors are increased to 40%.

Although flow evolution is present in the Beltrami pseudo-observations (10-min e-folding decay time) but not accounted for in the vorticity constraint, the neglect
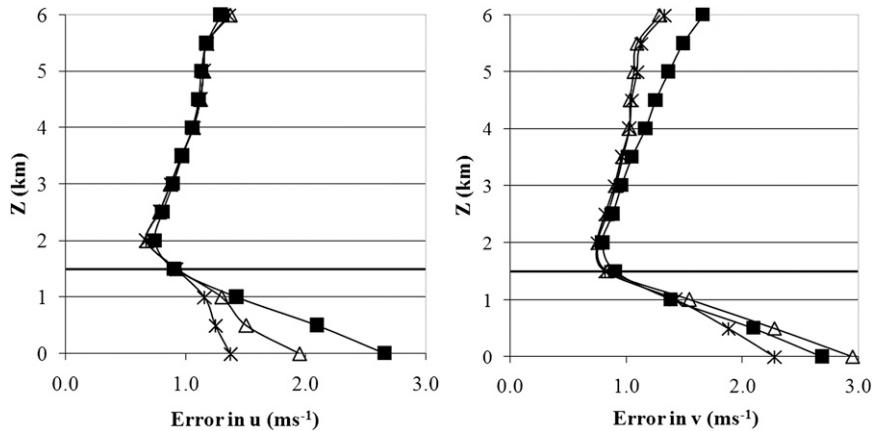
FIG. 3. Vertical profiles of the RMSEs in u and v for experiments IMP (squares), VORT (triangles), and IMP + VORT (stars). Parameter settings are given in section 5. The RMS values of u and v in the exact solution are ~10 m s^{-1} at every level.

of both flow evolution and diffusion in the vorticity constraint creates an artificially optimistic situation. This is because Beltrami flows have the unusual property that diffusion of vorticity exactly balances the part of the local derivative associated with flow evolution (the two terms sum to zero in the Beltrami model and are individually zero in our analysis vorticity constraint). However, spatial interpolation errors in the Cressman step; spatial-discretization errors in the mass conservation and vorticity equation constraints; random observational errors; failure to account for flow evolution in the data constraint; and (especially) the systematic errors in U and V, which impact both the spatial shift of data in the data constraint and the accuracy of the local derivative term in the vorticity constraint, should help counter the identical twin problem in our experiments.

6. Results

In the experiments described herein, radial wind pseudo-observations at heights less than 1.5 km AGL are withheld from the analysis. The same data, smoothness, and mass conservation constraints are imposed in all experiments. To allow the impermeability condition to influence the flow in the region of data coverage, the mass conservation and smoothness constraints are used everywhere—even in the regions of missing data. This mode of applying the mass conservation and smoothness constraints was used in all experiments, even in the experiments where the impermeability condition was not imposed. In the experiments in which the vorticity equation constraint is imposed, it is also imposed everywhere. In all experiments, the lowest analysis level is the ground surface ($z = 0$).

The experiments differ primarily in the application of the impermeability condition and in the use of the vorticity equation constraint. In experiment IMP, the impermeability condition is imposed without the vorticity equation constraint. In experiment VORT, the vorticity equation constraint is imposed without the impermeability condition. In experiment IMP + VORT, both the impermeability condition and the vorticity equation constraint are imposed.

As seen in Figs. 3 and 4, the root-mean-square errors (RMSEs) in each of the three wind components are
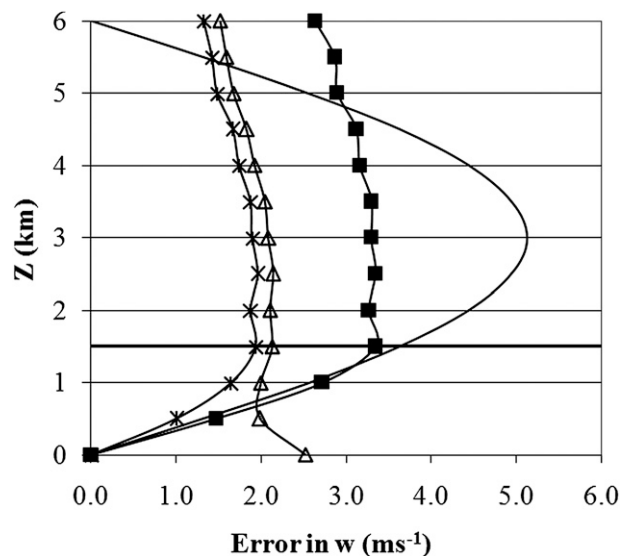

FIG. 4. Vertical profiles of the RMSE in w for experiments IMP (squares), VORT (triangles), and IMP + VORT (stars). For reference, the RMS value of w from the exact solution is also presented (solid line without plotting symbols). Parameter settings are given in section 5.
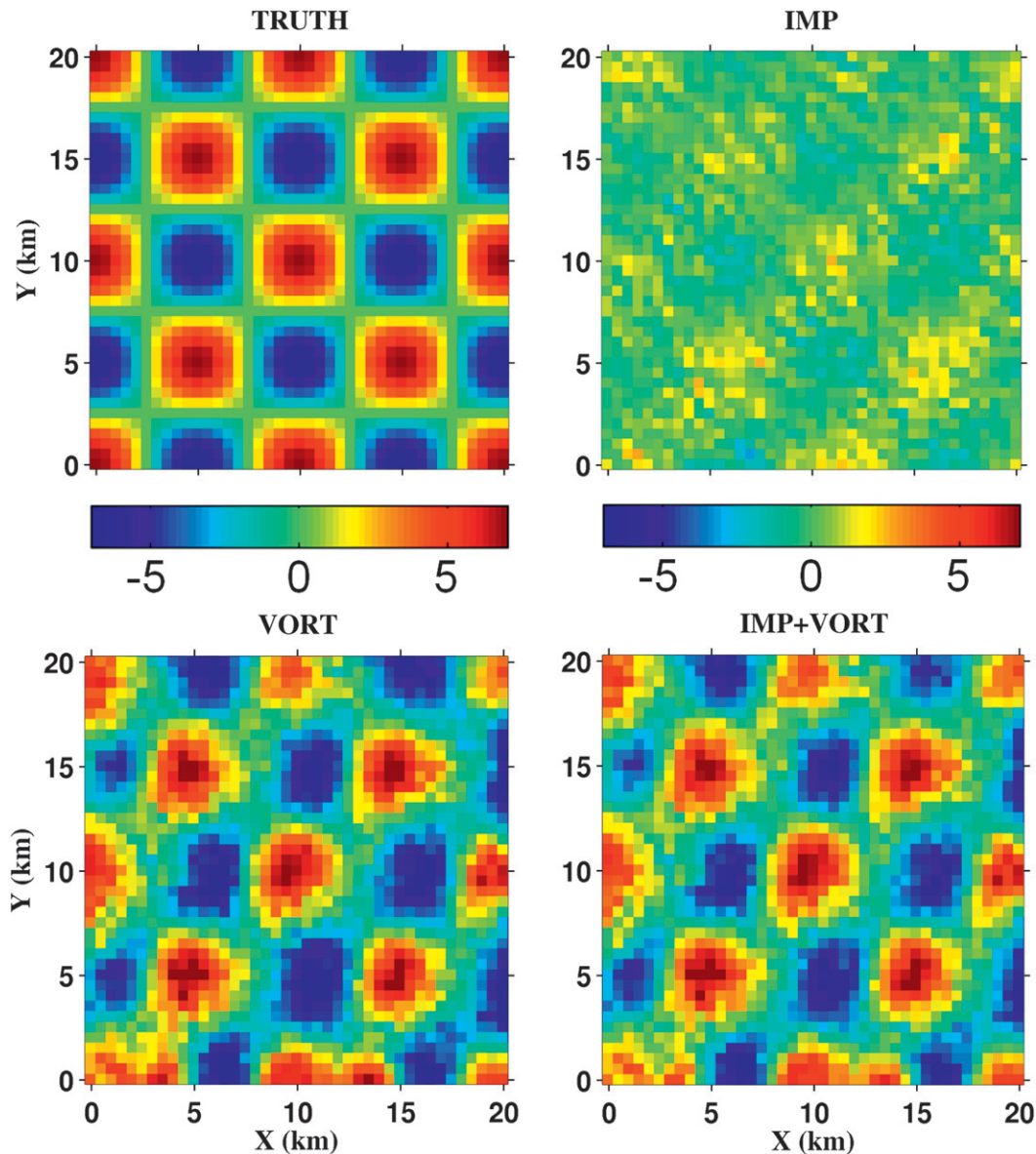
FIG. 5. Horizontal cross section of the vertical velocity field w (m s^{-1}) at $z = 1.5$ km for (top left) the exact solution and (top right) experiments IMP, (bottom left) VORT, and (bottom right) IMP + VORT. Parameter settings are given in section 5.

lower at every level in experiment IMP + VORT than in experiment IMP. The improvements are most significant for the vertical velocity component. Evidently the vertical vorticity constraint is providing useful dynamical information in the region of data coverage. Horizontal and vertical cross sections of the vertical velocity field in these experiments (Figs. 5 and 6) show that the intensities of the updrafts and downdrafts are greatly underestimated in experiment IMP. The IMP analysis is unable to recover from the large volume of missing information about the low-altitude convergence and

divergence. In contrast, in experiments VORT and IMP + VORT, the dynamical information provided by the vorticity equation in the region of data coverage provides a mechanism to build back the peak magnitudes of the vertical velocity field. Visually, the w cross sections in VORT and IMP + VORT are quite similar, but the error plots (Figs. 3 and 4) confirm that IMP + VORT yields slightly better results. Figures 5 and 6 suggest that, although some of the error in the analyzed w field in VORT and IMP + VORT is due to the w field being slightly too weak (though greatly improved from
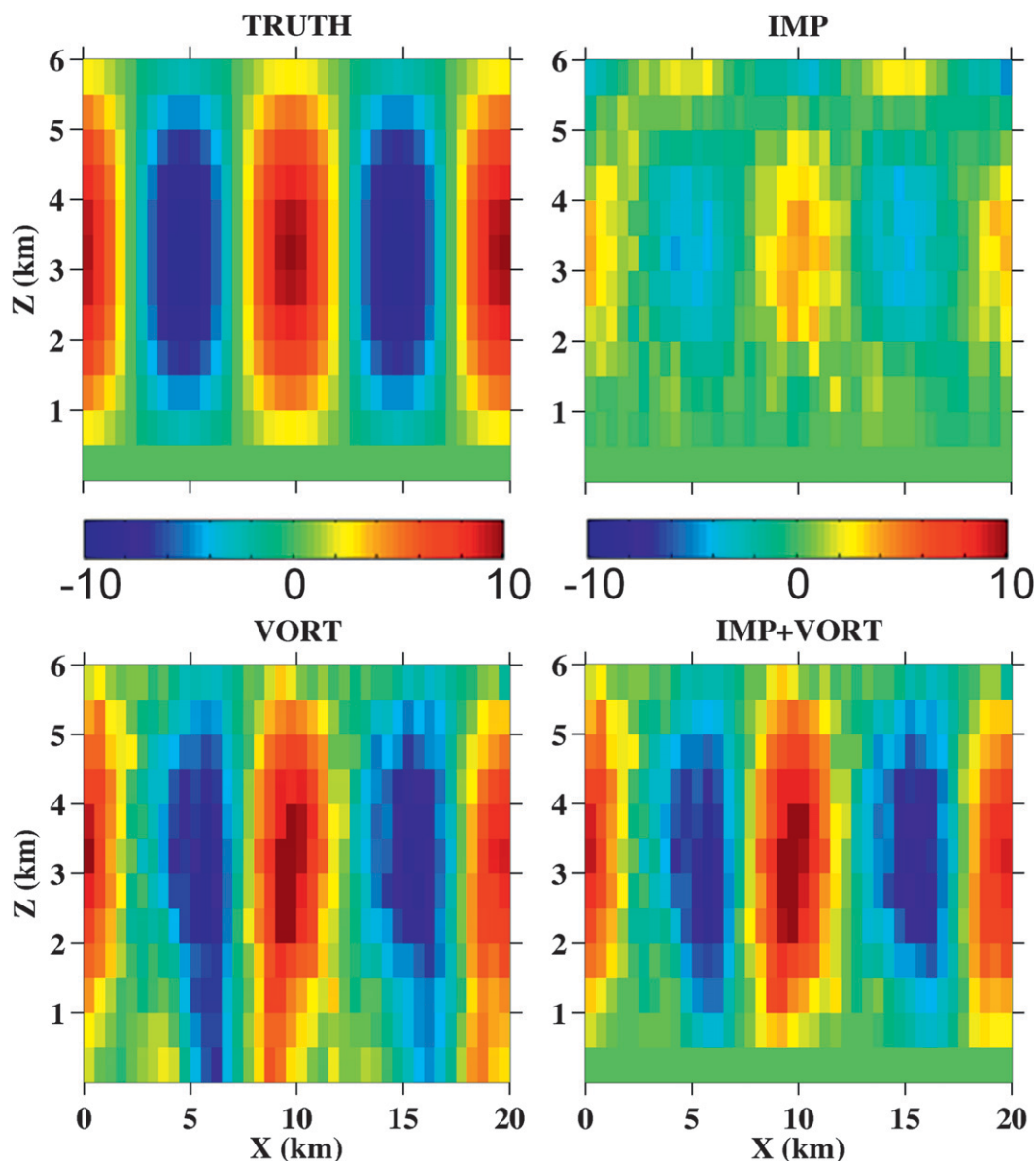
FIG. 6. As in Fig. 5, but for a vertical cross section of the vertical velocity field w (m s^{-1}) at $y = 10$ km.

IMP), most of the error is associated with noisiness in the analyzed field.

An additional set of experiments explored the sensitivity of the procedure to the values of the weighting coefficients. Because the radars were scanning at relatively low elevation angles, the horizontal part of the velocity vector was well sampled but the vertical part was largely unobserved. Accordingly, of the three Cartesian wind components, the vertical component was the most sensitive to changes in the analysis weights. Fortunately, as shown in Table 1, we found a large range of data, mass conservation, and vorticity constraint weights over which even this most sensitive wind component did

not change appreciably. The vertical velocity exhibited the greatest sensitivity to the smoothness weight.

Next, a series of experiments was conducted to determine the sensitivity of the analysis to the length of the analysis time window. Figure 7 depicts the relative root-mean-square error in w at the 1.5-km level for experiments in which the volume scan time ranges from 1 min (typical of scan periods from field deployments of research radars) to 5 min [characterizing the operational scan period of Weather Surveillance Radar-1988 Doppler (WSR-88D) radars]. For every volume scan period tested, VORT provided a better analysis of w than IMP, but the best results were obtained in IMP + VORT. However,

TABLE 1. RMSE in w expressed as a percentage of the RMS w from the exact solution at the 1.5- and 3.0-km levels for the weighting-coefficient sensitivity experiments. In each of these experiments, one weight is varied, whereas the others are fixed at the default values $C_O = 1$, $C_M = 0.1$, $C_V = 7.0 \times 10^{-4}$, and $C_S = 5.6 \times 10^{-5}$. Radial winds from one 2-min volume scan are used from each radar. These data are contaminated with random error, and U and V pattern-translation components are contaminated with 20% systematic error. See section 5 for complete parameter settings and other details.

	RMSE (%) in w at 1.5 km AGL			RMSE (%) in w at 3 km AGL		
	IMP	VORT	IMP + VORT	IMP	VORT	IMP + VORT
$1/10 \times C_O$	92.7	73.5	60.8	69.6	51.4	44.5
$1/3 \times C_O$	92.0	64.9	55.3	65.5	44.0	38.0
C_O	92.3	58.8	53.3	64.3	40.7	37.0
$3 \times C_O$	94.4	62.3	58.4	64.8	42.9	40.2
$10 \times C_O$	99.2	75.4	72.0	66.8	50.5	48.2
$0.0001 \times C_M$	98.5	64.3	60.1	95.8	84.0	83.2
$0.01 \times C_M$	92.0	61.2	53.9	68.1	47.3	43.8
C_M	92.3	58.8	53.3	64.3	40.7	37.0
$100 \times C_M$	93.5	56.7	52.7	65.3	39.9	36.6
$10\,000 \times C_M$	106.8	115.6	106.7	92.6	88.5	92.7
$1/10 \times C_V$	—	77.5	73.2	—	54.8	51.5
$1/3 \times C_V$	—	61.0	58.9	—	43.4	42.0
C_V	—	58.8	53.3	—	40.7	37.0
$3 \times C_V$	—	87.2	72.8	—	58.6	48.4
$10 \times C_V$	—	122.4	106.8	—	99.8	92.7
$1/10 \times C_S$	99.5	133.6	118.7	66.8	91.6	86.5
$1/3 \times C_S$	94.5	76.9	72.2	64.8	52.1	47.8
C_S	92.3	58.8	53.3	64.3	40.7	37.0
$3 \times C_S$	92.0	61.6	58.7	65.6	44.5	42.4
$10 \times C_S$	92.8	82.6	78.1	69.9	62.2	59.2

Fig. 7 also reveals an ominous trend: the tendency for a steeper degradation of performance with increased volume scan time in the VORT and IMP + VORT experiments than in the IMP experiment. Evidently, the vorticity equation constraint, though still adding value to the analysis, is beginning to exhibit sensitivity to errors in the frozen-turbulence hypothesis (recall that the U and V pattern-translation components used in the analysis tests were contaminated with 20% systematic error and that the pseudo-observations were generated with a 10-min e-folding decay time). As a follow-up experiment, we repeated these volume scan time experiments with systematic errors in the U and V pattern-translation components increased to 40% ($U = 6\,\text{m s}^{-1}$ and $V = 14\,\text{m s}^{-1}$ compared with correct values of 10 and 10 m s^{-1}, respectively). As seen in Fig. 8, these experiments reveal a significant deterioration of the performance of the vorticity equation–based experiments VORT and IMP + VORT. In this case, IMP provides better results than VORT or IMP + VORT when used with data from 3-, 4-, or 5-min volume scans. The vorticity constraint is still able to improve the analysis when data are gathered in a "rapid scan" mode, with IMP + VORT yielding the best results with data from 1- and 2-min volume scans, but the improvement over IMP is only marginal.

In a set of experiments designed to further explore the sensitivity of the analysis to length of the analysis time window, we fixed the volume scan period at 2 min (and reverted back to the 20% systematic error in U and V estimates used in the majority of our experiments) but varied the number of volume scans. Table 2 indicates that IMP, VORT, and IMP + VORT all degrade as multiple volume scans are used, but IMP + VORT yields the best results, even in the three-scan case where use of the vorticity equation by itself (VORT) proved disastrous. A follow-on experiment (also shown in Table 2) where three scans were used but the temporal-decay term in the specification of the pseudo-observations was turned off yielded much improved results. Contrasting this latter unrealistically optimistic experiment with the other, more realistic, three-scan experiments highlights the danger of degraded retrieval accuracy when long time windows are used with (inevitably) evolving wind fields. However, the results from the two-scan experiments (Figs. 7 and 8) suggest that the impact of flow evolution can be partially mitigated if data are available in a rapid-scan mode. Presumably, the improvement brought about by rapid scanning comes from a more accurate discrepancy calculation (shifting of analyzed winds) used in the evaluation of (9).

Table 3 summarizes results from experiments designed to systematically explore the relative impacts of the various sources of error. In these experiments, radial winds from one 2-min volume scan are used from each
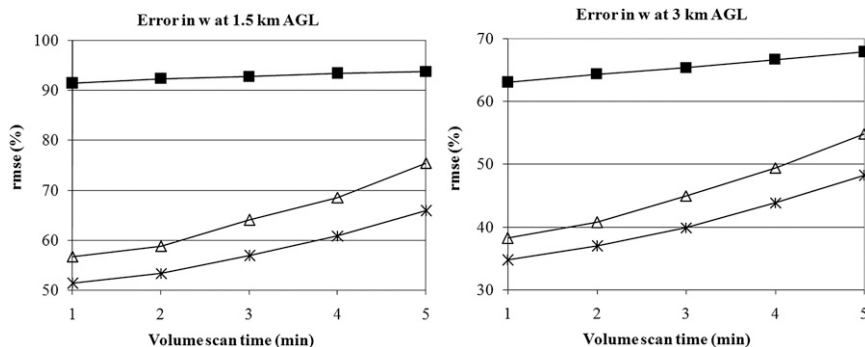
FIG. 7. RMSE in *w* expressed as a percentage of the RMS *w* from the exact solution for the volume scan time experiments. Results are shown for the 1.5- and 3-km levels for experiments IMP (squares), VORT (triangles), and IMP + VORT (stars). Complete parameter settings are given in section 5.

radar. The "no" data cutoff experiments are run with radial wind data available throughout the analysis domain. The "yes" data cutoff experiments are run with radial wind data withheld at heights beneath 1.5 km. In the "no" decay term experiments, the temporal-decay term in the Beltrami solution used to generate the pseudo-observations is turned off. In the "no" v_r error experiments, random errors are not applied to the radial wind pseudo-observations. In the "no" U and V error experiments, the exact U and V pattern-translation components are used (20% errors are imposed in the "yes" experiments). The experiments in the first row (no, no, no, and no) are the most optimistic; the only errors are the inevitable "procedural" errors associated with the Cressman interpolation step, the spatial discretizations of the mass conservation and vorticity equation constraints, and the imposition of the smoothness constraint. The experiments in the second row (yes, no, no, and no) differ from those in the first row in that data are now withheld for $z < 1.5$ km. In this case, the quality of the IMP, VORT, and IMP + VORT retrievals degrade, but the

degradation is far more serious for IMP than for VORT or IMP + VORT. Indeed, the errors in IMP have apparently saturated, with only minor increases in IMP retrieval errors as further sources of error are brought in. The experiments of the third row (yes, yes, no, and no) show that, when the pseudo-observations are allowed to evolve, the retrievals in which the vorticity constraint is used (VORT and IMP + VORT) degrade by an additional 8%. Compared to the third row experiments, a further 6% degradation in VORT and IMP + VORT is evident in the fourth row experiments (yes, yes, yes, and no), in which random observational errors are accounted for. However, a more pronounced degradation of VORT and IMP + VORT is evident when errors in the pattern-translation components are accounted for (cf. the fifth row experiments to the fourth row experiments). Once the pattern-translation error has been accounted for, imposition of random observational error (sixth row experiments) has only a minor impact on VORT or IMP + VORT (although, curiously, VORT actually undergoes a very slight improvement).
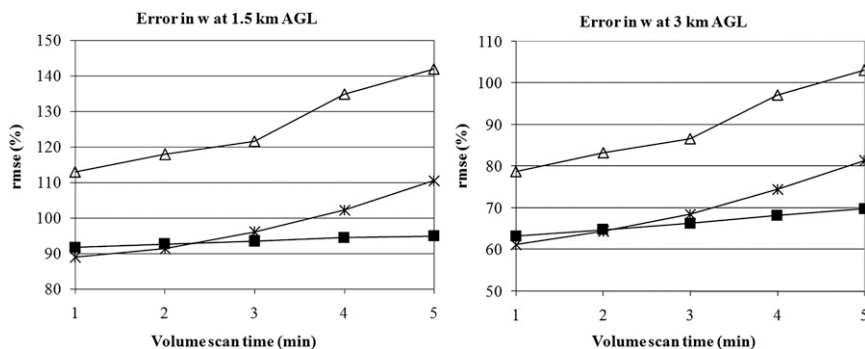

FIG. 8. As in Fig. 7, but for experiments in which the systematic errors imposed in the *U* and *V* pattern-translation components were increased from 20% to 40%.

TABLE 2. RMSE in w expressed as a percentage of the RMS w from the exact solution at the 1.5- and 3.0-km levels for the multiple sequential volume scans experiments. Each scan takes 2 min to complete. In the last experiments (no decay), the exponential temporal-decay term in the specification of the pseudo-observations was turned off.

	RMSE (%) in w at 1.5 km AGL		
	IMP	VORT	IMP + VORT
1 scan	92.3	58.8	53.3
2 scans	118.2	223.5	81.5
3 scans	187.8	616.1*	150.3
3 scans, no decay	81.1	62.7	52.0
	RMSE (%) in w at 3 km AGL		
	IMP	VORT	IMP + VORT
1 scan	64.3	40.7	37.0
2 scans	81.2	150.1	56.3
3 scans	123.7	424.0*	99.7
3 scans, no decay	56.3	47.4	41.1

* An experiment in which the convergence was particularly slow; these experiments were terminated with the (stringent) convergence criterion not quite being met.

A special concern for those interested in using results from a weak-constraint dual-Doppler analysis in further quantitative analysis is the extent to which the mass conservation equation is violated. To see how this constraint is violated in our experiments (recall that in our experiments the constraining mass conservation equation was the incompressibility condition), we calculate a normalized divergence defined on each analysis level z as the ratio of the RMS velocity divergence to the root of the mean of the sum of the squares of the three terms comprising the velocity divergence. Figure 9 depicts vertical profiles of this normalized divergence for IMP, VORT, and IMP + VORT for the same experiments considered in Figs. 3–6. Not surprisingly, the normalized divergence is larger in the VORT and IMP + VORT experiments than in the IMP experiment, because minimization of a vorticity constraint would generally be at some expense to other constraints. However, even in these VORT and IMP + VORT experiments, the nor-

malized divergence is very small: less than 0.005 at all levels. We also inspected horizontal cross sections (not shown) of a local normalized divergence, which is defined as the ratio of the velocity divergence to the root of the sum of the squares of the three terms comprising the velocity divergence. Although this local normalized divergence was less than 0.01 throughout much of the domain, there were isolated points where it was as large as 0.2–0.4. However, these isolated points were all found to be associated with very small values of each of the terms comprising the divergence, so the absolute (not normalized) divergence was very small. We conclude that even though mass conservation is imposed as a weak constraint, it is being very well satisfied throughout the analysis domain.

In a final set of experiments, we considered a Beltrami test case similar to that used in the previous experiments but with the vertical wavelength doubled [m halved to $2\pi/(24\text{ km})$]. The w field in this new test case attains a maximum value at the top of the analysis domain, instead of in the middle of it, and the low-level horizontal divergence is weaker than in the original case. As seen in Fig. 10, the IMP + VORT retrieval still yields superior results at every level. However, compared to the old test case (Fig. 4), the performance of VORT is now worse than IMP at every level. Part of this reversal is due to the improved performance of IMP with the new wind field. This improvement is not surprising, because the new wind field is characterized by a weaker low-level horizontal divergence and so the omission of the winds in the data void region impacts IMP less than it did with the original wind field. However, the other contributing factor to the reversal of the performance is the degradation of the results in the VORT experiment. We are still trying to understand the reason for this degradation. One explanation may be related to the fact that doubling the vertical wavelength of the input winds weakens both the wind shear and the horizontal divergence (which appear in the tilting and stretching terms in the vorticity equation) by factors of 2. This reduction may reduce the effectiveness of the vorticity equation as a constraint

TABLE 3. RMSE in w expressed as a percentage of the RMS w from the exact solution for experiments with various sources of error. Results are shown for the $z = 1.5$ km level. See text for description of the experiments.

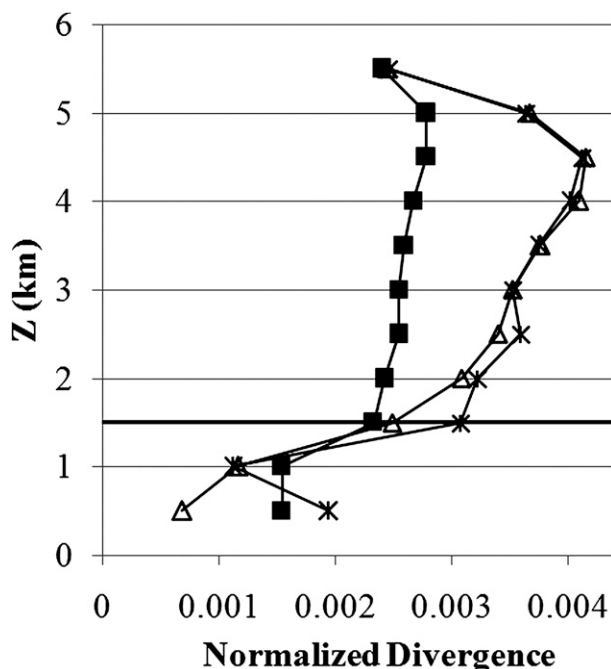| Error sources				RMSE in w (%) at 1.5 km		
Data cutoff	Decay term	ν_r error	U, V error	IMP	VORT	IMP + VORT
No	No	No	No	25.5	15.6	12.5
Yes	No	No	No	89.3	30.6	32.7
Yes	Yes	No	No	90.3	39.3	40.8
Yes	Yes	Yes	No	91.7	45.3	46.2
Yes	Yes	No	Yes	90.8	60.9	53.1
Yes	Yes	Yes	Yes	92.3	58.8	53.3

FIG. 9. Vertical profile of the normalized three-dimensional velocity divergence for the IMP (squares), VORT (triangles), and IMP + VORT (stars) experiments considered in Figs. 3–6.
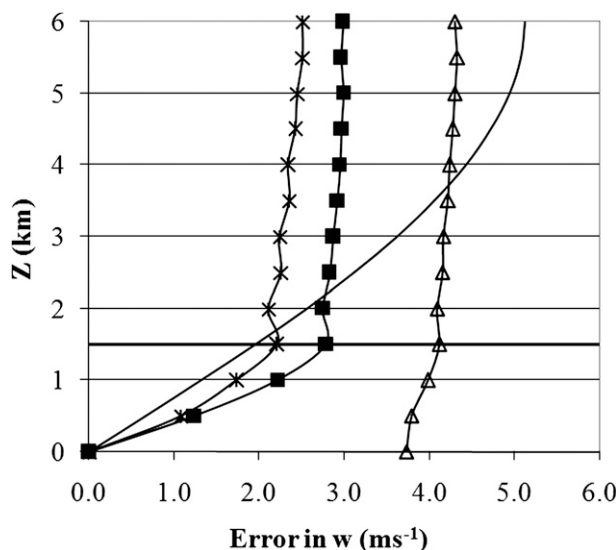

FIG. 10. As in Fig. 4, but for a test case in which the vertical wavelength of the pseudo-observations is twice that considered in the previous experiments.

in a manner analogous to the reduced effectiveness of scalar conservation equations in single-Doppler velocity retrieval in regions where the gradient of the scalar becomes weak (e.g., Qiu and Xu 1992; Shapiro et al. 1995; Lazarus et al. 1999). Fortunately, despite the poor performance of the VORT retrieval, the VORT + IMP experiment shows that the vorticity constraint still adds value when it is combined with the impermeability condition.

7. Summary and conclusions

We have explored the utility of the anelastic vertical vorticity equation as a weak constraint in a variational dual-Doppler analysis procedure that also incorporates traditional constraints (data, mass conservation, and smoothness) and the frozen-turbulence hypothesis. Our focus was on the value added by the vorticity equation constraint in cases where radars fail to sample low levels of the atmosphere. The procedure was tested with pseudo-observations of a Beltrami flow solution of the Navier–Stokes equations describing a translating and temporally decaying array of counterrotating updrafts and downdrafts. Data were contaminated with random error, whereas systematic errors were imposed on the estimated U and V frozen-turbulence pattern-translation components. Data from heights <1.5 km AGL were withheld from the analysis to simulate the low-level data

coverage problem. Three types of data-denial experiments were performed: the impermeability condition imposed without a vorticity equation constraint, the vorticity equation constraint imposed without the impermeability condition, and both the impermeability condition and the vorticity equation constraint imposed.

In the default experiment configuration (parameters given in section 5), the test without the vorticity equation showed that the traditional constraints by themselves were unable to compensate for missing data that contained information about the highly convergent/divergent low-level flow. In contrast, the vorticity constraint provided useful dynamical information about the vertical velocity field in the region of data coverage that greatly improved the analysis. The best results were obtained when both the impermeability condition and vorticity constraint were imposed.

In experiments with volume scan periods ranging from 1 to 5 min, the vorticity equation constraint was again found to add value, but the effect was diminished at the longer scan periods. When these experiments were repeated with systematic errors in the estimated pattern-translation components doubled (40% error), the vorticity equation constraint degraded the accuracy of the retrieval when the longer-period volume scans were used but added value when the shorter-period scans were used, provided the impermeability condition was also applied. These and related experiments focusing on the use of multiple volume scans suggest that the vorticity equation can provide useful dynamical information but only if the pattern-translation components

are estimated sufficiently accurately and the analysis time window is kept short. Errors stemming from inaccurate estimates of the pattern-translation components (or breakdown of the frozen-turbulence hypothesis itself) can be mitigated by the use of rapid-scan data. However, it should be kept in mind that our tests were performed in an idealized analytical framework (see especially the last paragraph of section 5) and that extensive tests with real data should be undertaken before general conclusions can be drawn. We have recently begun tests of the algorithm with a real supercell dataset.

Based on results from the experiments described herein and from the "vorticity method" studies cited in section 1, we anticipate that the greatest challenge to a wider application of a vertical vorticity equation constraint in dual-Doppler analysis systems is to ensure a sufficiently accurate discretization of the local derivative term. Improvements in the treatment of that term might be made on several fronts. First, because storm environments are typically sheared and different parts of storms may move at different speeds, it might be necessary to work with spatially variable U and V pattern-translation components rather than the constant values used in traditional space-to-time conversions. Toward that end, a recently developed advection-correction algorithm that estimates spatially variable pattern-translation components from reflectivity data (manuscript in preparation) might prove useful. It might also be necessary to account for intrinsic evolution effects (unsteadiness in a moving reference frame). Approaches described by Protat and Zawadzki (2000), Protat et al. (2001), and Liu et al. (2004) might be beneficial for that purpose. In addition, as new generations of Doppler radar platforms come online, rapid-scan datasets of a variety of mesoscale phenomena are becoming increasingly available for dual-Doppler wind analysis. Among the radar systems that can provide rapid-scan data are phased array weather radars (Zrnic et al. 2007); dense networks of low-cost, low-power radars with flexible scanning strategies, such as those developed by the Engineering Research Center for the Collaborative Adaptive Sensing of the Atmosphere (CASA; Brotzge et al. 2006); and mobile Doppler radars, such as the Shared Mobile Atmospheric Research and Teaching Radar (SMART-R; Biggerstaff et al. 2005), the Doppler-on-Wheels (DOW; Wurman et al. 1997), and the University of Massachusetts mobile Doppler radar (Bluestein and Pazmany 2000).

REFERENCES

Anagnostou, E. N., and W. Krajewski, 1999: Real-time radar rainfall estimation. Part I: Algorithm formulation. *J. Atmos. Oceanic Technol.,* **16,** 189–197.

Austin, G. L., and A. Bellon, 1974: The use of digital weather radar records for short-term precipitation forecasting. *Quart. J. Roy. Meteor. Soc.,* **100,** 658–664.

Bannon, P. R., 1996: On the anelastic approximation for a compressible atmosphere. *J. Atmos. Sci.,* **53,** 3618–3628.

Biggerstaff, M. I., and Coauthors, 2005: The shared mobile atmospheric research and teaching radar: A collaboration to enhance research and teaching. *Bull. Amer. Meteor. Soc.,* **86,** 1263–1274.

Bluestein, H. B., and A. L. Pazmany, 2000: Observations of tornadoes and other convective phenomena with a mobile, 3-mm wavelength, Doppler radar: The spring 1999 field experiment. *Bull. Amer. Meteor. Soc.,* **81,** 2939–2951.

Brotzge, J. A., K. Droegemeier, and D. J. McLaughlin, 2006: Collaborative adaptive sensing of the atmosphere: New radar system for improving analysis and forecasting of surface weather conditions. *J. Transport. Res. Board,* **1948,** 145–151.

Caillault, K., and Y. Lemaître, 1999: Retrieval of three-dimensional wind fields corrected for the time-induced advection problem. *J. Atmos. Oceanic Technol.,* **16,** 708–722.

Caya, A., S. Laroche, I. Zawadzki, and T. Montmerle, 2002: Using single-Doppler data to obtain a mesoscale environmental field. *J. Atmos. Oceanic Technol.,* **19,** 21–36.

Chong, M., J. Testud, and F. Roux, 1983: Three-dimensional wind field analysis from dual-Doppler radar data. Part II: Minimizing the error due to temporal variation. *J. Climate Appl. Meteor.,* **22,** 1216–1226.

Collins, G. O., and P. M. Kuhn, 1954: A generalized study of precipitation forecasting. Part 3: Computation of precipitation resulting from vertical velocities deduced from vorticity changes. *Mon. Wea. Rev.,* **82,** 173–182.

Daley, R., 1991: *Atmospheric Data Analysis.* Cambridge University Press, 457 pp.

Debrant, G., and Ph. Wehrlé, 1935: L'équation du tourbillon synoptique et son application à la théorie du système nuageux. Union Géodésique et Géophysique Internationale Cinquième Assemblée Générale. Lisbonne 1933. *P.-V. Séances Assoc. Météorologie,* **2,** 117–144.

Doviak, R. J., and D. S. Zrnic, 1984: *Doppler Radar and Weather Observation.* Academic Press, 458 pp.

——, P. S. Ray, R. G. Strauch, and L. J. Miller, 1976: Error estimation in wind fields derived from dual-Doppler radar measurement. *J. Appl. Meteor.,* **15,** 868–878.

Dowell, D. C., C. R. Alexander, J. M. Wurman, and L. J. Wicker, 2005: Centrifuging of hydrometeors and debris in tornadoes: Radar reflectivity patterns and wind measurement errors. *Mon. Wea. Rev.,* **133,** 1501–1524.

Dutton, J. A., and G. H. Fichtl, 1969: Approximate equations of motion for gases and liquids. *J. Atmos. Sci.,* **26,** 241–254.

Eliassen, A., and W. E. Hubert, 1953: Computations of vertical motion and vorticity budget in a blocking situation. *Tellus,* **5,** 196–206.

Fuelberg, H. E., and T. W. Funk, 1987: Diagnosis of vertical motion from VAS retrievals. *J. Climate Appl. Meteor.,* **26,** 1655–1670.

Gal-Chen, T., 1982: Errors in fixed and moving frame of references: Applications for conventional and Doppler radar analysis. *J. Atmos. Sci.,* **39,** 2279–2300.

Gao, J., M. Xue, A. Shapiro, and K. K. Droegemeier, 1999: A variational method for the analysis of three-dimensional wind fields from two Doppler radars. *Mon. Wea. Rev.,* **127,** 2128–2142.

Haltiner, G. J., and R. T. Williams, 1980: *Numerical Prediction and Dynamic Meteorology.* 2nd ed. John Wiley and Sons, 477 pp.

Heymsfield, G. M., 1978: Kinematic and dynamic aspects of the Harrah tornadic storm analysed from dual-Doppler radar data. *Mon. Wea. Rev.,* **106,** 233–254.

Hoffman, R. N., 1984: SASS wind ambiguity removal by direct minimization. Part II: Use of smoothness and dynamical constraints. *Mon. Wea. Rev.,* **112,** 1829–1852.

Irmay, S., and M. Zuzovsky, 1970: Exact solutions of the Navier-Stokes equations in two-way flows. *Israel J. Technol.,* **8,** 307–315.

Kropfli, R. A., and L. J. Miller, 1976: Kinematic structure and flux quantities in a convective storm from dual-Doppler radar observations. *J. Atmos. Sci.,* **33,** 520–529.

Lazarus, S., A. Shapiro, and K. Droegemeier, 1999: Analysis of the Gal-Chen–Zhang single-Doppler velocity retrieval. *J. Atmos. Oceanic Technol.,* **16,** 5–18.

——, ——, and ——, 2001: Application of the Zhang-Gal-Chen single-Doppler velocity retrieval to a deep convective storm. *J. Atmos. Sci.,* **58,** 998–1016.

Lee, J. L., and G. L. Browning, 1994: Analysis of errors in the horizontal divergence derived from high temporal resolution of the wind. *Mon. Wea. Rev.,* **122,** 851–863.

——, ——, and Y. F. Xie, 1995: Estimating divergence and vorticity from the wind profiler network hourly wind measurements. *Tellus,* **47A,** 892–910.

——, Y.-H. Kuo, and A. E. MacDonald, 2003: The vorticity method: Extension to mesoscale vertical velocity and validation for tropical storms. *Quart. J. Roy. Meteor. Soc.,* **129,** 1029–1050.

——, W. C. Lee, and A. E. MacDonald, 2006: Estimating vertical velocity and radial flow from Doppler radar observations of tropical cyclones. *Quart. J. Roy. Meteor. Soc.,* **132,** 125–145.

Liou, Y.-C., and I.-S. Luo, 2001: An investigation of the moving-frame single-Doppler wind retrieval technique using Taiwan area mesoscale experiment low-level data. *J. Appl. Meteor.,* **40,** 1900–1917.

Lipps, F. B., and R. S. Hemler, 1982: A scale analysis of deep moist convection and some related numerical calculations. *J. Atmos. Sci.,* **39,** 2192–2210.

Liu, S., C. Qiu, Q. Xu, and P. Zhang, 2004: An improved time interpolation for three- dimensional Doppler wind analysis. *J. Appl. Meteor.,* **43,** 1379–1391.

——, ——, ——, ——, J. Gao, and A. Shao, 2005: An improved method for Doppler wind and thermodynamic retrievals. *Adv. Atmos. Sci.,* **22,** 90–102.

Mateja, T., 2002: Estimating the most steady frame of reference from Doppler radar data. *J. Atmos. Oceanic Technol.,* **19,** 1035–1048.

Mewes, J. J., and A. Shapiro, 2002: Use of the vorticity equation in dual-Doppler analysis of the vertical velocity field. *J. Atmos. Oceanic Technol.,* **19,** 543–567.

Miller, A., and H. A. Panofsky, 1958: Large-scale vertical motion and weather in January, 1953. *Bull. Amer. Meteor. Soc.,* **39,** 8–13.

Nash, W. P., and L. W. Chamberlain, 1954: Some aspects of the heavy rains in the Chicago area, October 9-11, 1954. *Mon. Wea. Rev.,* **82,** 305–316.

Press, W. H., S. A. Teukolsky, W. T. Vetterling, and B. P. Flannery, 1992: *Numerical Recipes in FORTRAN: The Art of Scientific Computing.* 2nd ed. Cambridge University Press, 963 pp.

Protat, A., and I. Zawadzki, 2000: Optimization of dynamic retrievals from a multiple-Doppler radar network. *J. Atmos. Oceanic Technol.,* **17,** 753–760.

——, ——, and A. Caya, 2001: Kinematic and thermodynamic study of a shallow hailstorm sampled by the McGill bistatic multiple-Doppler radar network. *J. Atmos. Sci.,* **58,** 1222–1248.

Qiu, C.-J., and Q. Xu, 1992: A simple adjoint method of wind analysis for single-Doppler data. *J. Atmos. Oceanic Technol.,* **9,** 588–598.

——, and ——, 1996: Least squares retrieval of microburst winds from single-Doppler radar data. *Mon. Wea. Rev.,* **124,** 1132–1144.

Ray, P. S., 1976: Vorticity and divergence fields within tornadic storms from dual-Doppler observations. *J. Appl. Meteor.,* **15,** 879–890.

——, R. J. Doviak, G. B. Walker, D. Sirmans, J. Carter, and B. Bumgarner, 1975: Dual-Doppler observation of a tornadic storm. *J. Appl. Meteor.,* **14,** 1521–1530.

Riehl, H., K. S. Norquest, and A. L. Sugg, 1952: A quantitative method for the prediction of rainfall patterns. *J. Meteor.,* **9,** 291–298.

Sasaki, Y., 1970: Some basic formalisms in numerical variational analysis. *Mon. Wea. Rev.,* **98,** 875–883.

——, 1971: A theoretical interpretation of anisotropically weighted smoothing on the basis of numerical variational analysis. *Mon. Wea. Rev.,* **99,** 698–707.

Sawyer, J. S., 1949: Large scale vertical motion in the atmosphere. *Quart. J. Roy. Meteor. Soc.,* **75,** 185–188.

Scialom, G., and Y. Lemaître, 1990: A new analysis for the retrieval of three-dimensional mesoscale wind fields from multiple Doppler radar. *J. Atmos. Oceanic Technol.,* **7,** 640–665.

Shapiro, A., 1993: The use of an exact solution of the Navier-Stokes equations in a validation test of a three-dimensional non-hydrostatic numerical model. *Mon. Wea. Rev.,* **121,** 2420–2425.

——, 2005: Drag-induced transfer of horizontal momentum between air and raindrops. *J. Atmos. Sci.,* **62,** 2205–2219.

——, S. Ellis, and J. Shaw, 1995: Single-Doppler velocity retrievals with Phoenix II data: Clear air and microburst wind retrievals in the planetary boundary layer. *J. Atmos. Sci.,* **52,** 1265–1287.

Taylor, G. I., 1938: The spectrum of turbulence. *Proc. Roy. Soc. London,* **164A,** 476–490.

Thacker, W. C., 1988: Fitting models to inadequate data by enforcing spatial and temporal smoothness. *J. Geophys. Res.,* **93,** 10 655–10 665.

Truesdell, C., 1954: *The Kinematics of Vorticity.* Indiana University Press, 232 pp.

Wahba, G., and J. Wendelberger, 1980: Some new mathematical methods for variational objective analysis using splines and cross validation. *Mon. Wea. Rev.,* **108,** 1122–1143.

Wurman, J., J. Straka, E. Rasmussen, M. Randall, and A. Zahrai, 1997: Design and deployment of a portable, pencil-beam, pulsed, 3-cm Doppler radar. *J. Atmos. Oceanic Technol.,* **14,** 1502–1512.

Xu, Q., 2005: Representations of inverse covariances by differential operators. *Adv. Atmos. Sci.,* **22,** 181–198.

——, C.-J. Qiu, H.-D. Gu, and J.-X. Yu, 1995: Simple adjoint retrievals of microburst winds from single-Doppler radar data. *Mon. Wea. Rev.,* **123,** 1822–1833.

——, H. Gu, and C. Qiu, 2001: Simple adjoint retrievals of wet-microburst winds and gust-front winds from single-Doppler radar data. *J. Appl. Meteor.,* **40,** 1485–1499.

Yanai, M., and T. Nitta, 1967: Computation of vertical motion and vorticity budget in a Caribbean easterly wave. *J. Meteor. Soc. Japan,* **45,** 444–466.

Zawadzki, I. I., 1973: Statistical properties of precipitation patterns. *J. Appl. Meteor.,* **12,** 459–472.

Zrnic, D. S., and Coauthors, 2007: Agile-beam phased array radar for weather observations. *Bull. Amer. Meteor. Soc.,* **88,** 1753–1766.